ChemPubSoc Europe

DOI: 10.1002/chem.201304800

CHEMISTRY A European Journal Full Paper

Biosensors

Silica Nanowire Arrays for Diffraction-Based Bioaffinity Sensing

Gabriel Loget* and Robert M. Corn[a]

Abstract: Arrays of electrodeposited silica nanowires (SiO_2 NWs) have been fabricated over large areas (cm^2) on fluoropolymer thin films attached to glass substrates by a combination of photolithography and electrochemically triggered sol–gel nanoscale deposition. Optical and scanning electron microscopy (SEM) measurements revealed that the SiO_2 NW arrays had an average spacing of ten micrometers and an average width of 700 nm with a significant grain structure that was a result of the sol–gel deposition process. The optical diffraction properties at 633 nm of the SiO_2 NW arrays were characterized when placed in contact with solutions by using a prism-coupled total internal reflection geometry; quantification of changes in these diffraction properties was applied in various sensing applications. Bulk refractive index sensing by using the SiO_2 NW grating was demonstrated with a sensitivity of 1.30×10^{-5} RIU. Toposelectively chemically modified SiO_2 NW arrays were used for diffraction biosensing measurements of surface binding events, such as the electrostatic adsorption of gold nanoparticles and the bioaffinity adsorption of streptavidin onto a biotin monolayer. Finally, the application of the SiO_2 NW arrays for practical medical-diagnostic applications was demonstrated by monitoring the diffraction of SiO_2 NW arrays functionalized with a single-stranded (ss)DNA aptamer to detect human α-thrombin from solutions at sub-pathologic nanomolar concentrations.

Introduction

Light diffraction created by an optical interaction with periodic structures on surfaces is highly sensitive to the local interfacial properties of the scattering medium. This phenomenon has been used as the sensing principle for a number of simple, inexpensive, and label-free detection methods: pH measurements,[1] metal-deposition monitoring,[2] and the detection of volatile organic compounds,[3] DNA,[4,5] antibodies,[6–8] and bacteria.[9] Gratings formed from arrays of nanowires that exhibit unique optical and electrical properties have expanded the application of metallic and semiconductor gratings to include organic light-emitting diodes,[10] optical devices,[11] memristive memories,[12] capacitors,[13] mechanical resonators,[14] and sensors.[15] Metal,[16] metal-oxide,[13] and polymer[17] nanowire arrays can be fabricated by a variety of methods: focused ion-beam micromachining,[18] electron-beam lithography,[19] nanoimprint lithography,[20] superlattice nanowire pattern transfer,[21] and lithographically patterned electrodeposition (LPNE).[22,23] These nanowire arrays can be used for in situ measurements of surface reactions. For example, the optical diffraction from metal nanowires has been recently characterized[24] and employed for monitoring the electrodeposition of silver on gold.[2]

An alternative to metal nanowires for diffraction-grating sensor applications are silica nanowires (SiO_2 NWs). Recently, SiO_2 NWs have attracted great attention for applications in photonic devices due to their photoluminescence[25–28] and sub-wavelength guiding properties.[29–31] The processes reported to date for the synthesis of SiO_2 NWs are usually based on vapor-liquid/solid depositions,[32] oxidation of Si from a liquid alloy,[33] chemically triggered sol–gel process,[34] and drawing from bulk glass.[29] A drawback of these techniques is that they lead to the production of nanowire bundles[32–34] or individual freestanding nanowires,[29] which cannot be easily adapted to the formation of nanowire arrays for diffraction.

Herein, we report a new technique based on a modified LPNE[22,23] process, for the fabrication of SiO_2 NW arrays with high aspect ratio and roughness on a polymer layer (Cytop). The SiO_2 NWs were first characterized by optical and electron microscopy. The diffraction of the SiO_2 NW array was then studied by using total internal reflection (TIR) geometry and a 633 nm laser beam. We demonstrate the high sensitivity toward the changes in bulk refractive index by using these surfaces and show that surface modification can also be detected by electrostatically adsorbing gold nanoparticles (AuNPs) on the SiO_2 NWs. We then demonstrate the toposelective chemical biomodification of the SiO_2 NWs by fluorescence microscopy and use biotin-modified SiO_2 NWs to monitor the in situ binding of streptavidin. Finally, we functionalize the SiO_2 NWs with a single-stranded (ss)DNA aptamer for the detection of human α-thrombin at the nanomolar level.

[a] Dr. G. Loget, Prof. R. M. Corn
Department of Chemistry, University of California Irvine
Irvine, CA 92697 (USA)
E-mail: gabloget@yahoo.fr

Supporting information for this article is available on the WWW under http://dx.doi.org/10.1002/chem.201304800.

Results and Discussion

Fabrication of the silica nanowire arrays

The protocol used for the fabrication of the SiO_2 NW arrays on a fluoropolymer film (Cytop) consists of a modified LPNE process illustrated in Figure 1.

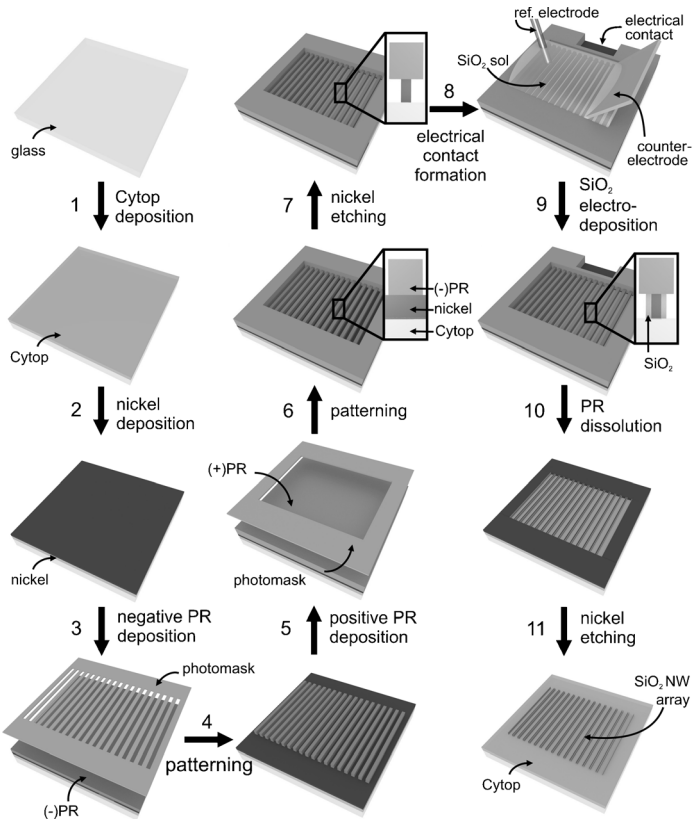

Figure 1. Schematic representation of the process used for the fabrication of SiO_2 NW arrays.

In the classical LPNE process developed by Penner and coworkers,[22,23] the use of a positive photoresist ((+)PR) is well suited for the electrodeposition of nanowires on glass in an aqueous media; it is not appropriate for the electrodeposition in electrolytes containing ethanol, because the (+)PRs are usually soluble in this solvent. Because sol–gel electrodeposition of silica is usually achieved in a water/ethanol mixture,[35–38] and because we wanted to fabricate the SiO_2 NWs on substrates other than glass slides, we adapted the LPNE technology to our needs by adding several steps to the process. First, a Cytop film with a thickness of approximately 40 nm was spin coated on a glass slide (step 1, Figure 1), and a 170 nm-thick nickel layer was then deposited on the Cytop by vapor deposition (step 2). An epoxy-based negative photoresist ((−)PR), SU-8 that is insoluble and resistant to the required solvents was deposited onto the nickel thin film (step 3) and used for patterning stripes with both a width and a spacing of 10 μm (step 4). A layer of (+)PR was then deposited on the surface (step 5) and developed (step 6) for protecting the nickel edges from the etching that will be performed in the following step, in order to preserve an electrical conduction pathway between the nickel stripes for the electrodeposition. The nickel was then etched with nitric acid 0.8 M for 14 min (step 7) to create nickel stripes with a width smaller than the width of the above (−)PR stripes. This way, two nanotrenches were created at both sides of the nickel stripe between the Cytop and the (−)PR layer (see inset of step 7). An electrical contact area was then made by dissolving a small part of the (+)PR edge with acetone (step 8).

In sol–gel approaches, a solid phase is formed through gelation of a colloidal suspension (sol).[39] The sol–gel deposition of SiO_2 coatings on conductive surfaces can be conveniently triggered by electrochemistry.[35–38] In this approach, a sol is first prepared by hydrolyzing a silica precursor (tetraethyl orthosilicate (TEOS)) in an ethanol/water mixture according to the following reaction [Eq. (1)]:

$$Si(OEt)_4 + 4\,H_2O \rightarrow Si(OH)_4 + 4\,EtOH \quad (1)$$

The silica sol is stable at pH 3. Next, a sufficiently negative potential is applied to the working electrode to induce proton evolution [Eq. (2)]:

$$2\,H^+ + 2\,e^- \rightarrow H_2 \quad (2)$$

The intense pH increase resulting from the consumption of the protons at the electrode surface triggers the polycondensation of the sol.[35–38] This polycondensation leads to the final SiO_2 coating on the electrode surface. As shown in Figure 1 (step 9), this sol–gel strategy was applied for the electrodeposition of silica onto the nickel confined in the nanotrenches. This was achieved by chronoamperometry at −1.2 V vs. Ag/AgCl (NaCl 3 M) for 70 s, by using the protected nickel substrate as a working electrode. The (+)PR was then dissolved by rinsing the surface with acetone and the (−)PR was removed by immersing the substrate into *N*-methylpyrrolidinone (NMP; step 10). Although NMP does not dissolve the (−)PR, it leads to its swelling and its detachment from the substrate over time.[40] Finally, the remaining nickel was etched (step 11), leading to the formation of the SiO_2 NW array on the Cytop film.

Characterization of the silica nanowire array

The SiO_2 NWs were characterized by a combination of optical microscopy and scanning electron microscopy (SEM). Figure 2 shows a large-area view obtained with an optical microscope that shows the SiO_2 NW array on the Cytop film.

The SiO_2 NWs can be clearly seen as long and straight clear-colored wires. In this picture, the length of the SiO_2 NWs exceeds 0.5 mm, and it was observed that the wires could be fabricated as long as a few millimeters. The height of the nanowires is controlled by the thickness of nickel layer, herein, 170 nm. The wire width is controlled by the electrodeposition time (Figure 1, step 9) and can be estimated from the inset of

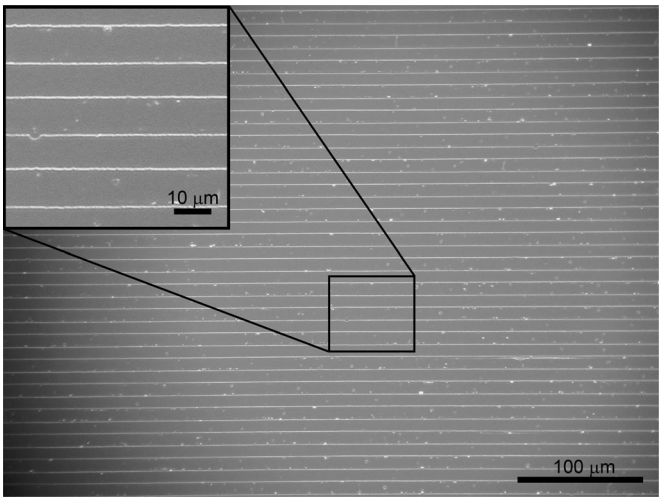

Figure 2. Optical micrograph showing a silica nanowire array. Inset: magnification of the squared area.

Figure 2 as 700 nm, which gives, based on the measurements achieved in this figure, an aspect ratio of 750. In reality, this aspect ratio value is much higher, because the length of the SiO_2 NWs exceeded the picture frame. The respective spacing between the wires is controlled by two parameters: 1) the width of the (−)PR stripes, which is 10 μm (Figure 1, step 4); and 2) the nickel etching time, which is 14 min (Figure 1, step 7). The spacing values can be measured from the inset of Figure 2. Because of the nickel etching step, which imparts an asymmetry to the array (Figure 1, step 7), two different values of 9 and 11 μm were measured. The smaller value corresponds to the distance between SiO_2 NWs deposited at the two sides of the same nickel stripe, and the higher value corresponds to the distance between SiO_2 NWs deposited at the facing sides of two neighboring nickel stripes. As shown in Figure 3, the SiO_2 NWs were further characterized by SEM. Figure 3a shows a section of a single SiO_2 NW, from which a width of 700 ± 90 nm was measured; this is in good agreement with the previously estimated width value determined by optical microscopy. Figure 3b shows a high resolution SEM picture of the surface of a SiO_2 NW, revealing that the SiO_2 surface exhibited a roughness at the nanometer scale. This important feature can be used advantageously in the context of biosensing by providing a high surface area, which will increase the biosensor sensitivity.

This process is very versatile in terms of dimensions of the fabricated nanowires and the following parameters: nickel-layer thickness, electrodeposition time, and width of the (−)PR stripes can be easily tuned to control the height, the width, and the spacing of the SiO_2 NWs, respectively. For example, SiO_2 NWs with widths of a few hundreds of nanometers could be obtained by using shorter electrodeposition times (Figure S1 in the Supporting Information). Importantly, the thickness layer was found to be a critical limiting parameter, as we found that discontinuous SiO_2 were obtained with nickel layers thinner than 100 nm (Figure S2 in the Supporting Information).

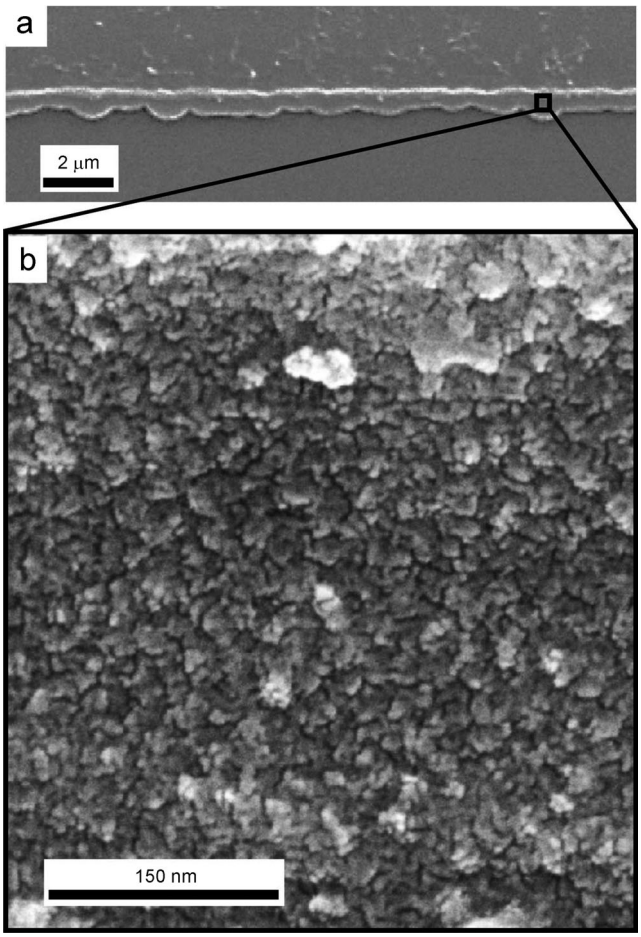

Figure 3. a) SEM picture of a section of a single silica nanowire. b) High magnification SEM picture showing the surface of a silica nanowire.

Characterization of the diffraction of the silica nanowire arrays

The diffraction of *p*-polarized visible light at a wavelength of $\lambda = 633$ nm by the SiO_2 NW array surface was characterized in water using the optical setup shown in Figure 4a. The glass slide of the SiO_2 NWs substrate was coupled to a glass prism with refractive index-matching fluid, positioned onto a rotating stage and the array surface was immersed with water by using a flow cell. The incident angle θ on the array surface was positioned beyond the critical angle so that the negative diffraction orders were in total internal reflection (TIR) geometry. The diffraction pattern was projected on a black screen and recorded by using a digital camera. The pattern is shown in the top of Figure 4b, the corresponding intensity profile is shown in the bottom part of Figure 4b. The image spot with the largest intensity corresponds to the reflection of the incoming light beam (indicated as zero order), whereas all the other spots correspond to different orders of diffraction. Of the twelve orders of diffraction shown herein, the spot corresponding to the −2 order reveals the highest intensity and therefore was used for the sensing experiments described in the following.

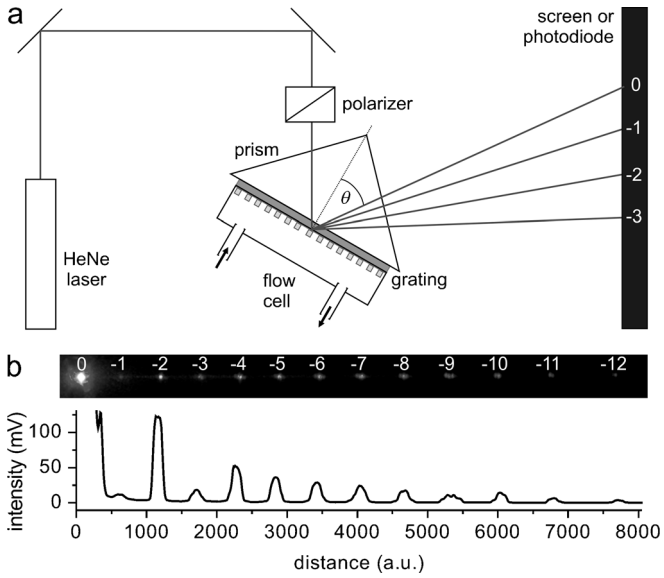

Figure 4. a) Set-up used for the analysis of the silica nanowire grating diffraction by using TIR geometry. b) Top: photograph of the diffraction pattern of a silica nanowire array taken in water. Bottom: corresponding intensity profile of the diffraction pattern.

Bulk refractive index sensing by using the silica nanowire array diffraction

The sensor characteristics were determined by studying the output signal, that is, the photodiode tension, as a function of the decreasing refractive index n of the solution injected into the flow cell. For these experiments, a photodiode was used to measure the intensity of the $n=-2$ diffraction order. The inset of Figure 5 shows the bulk refractive index detection curve, in which the difference of photodiode potential ΔE is plotted as a function of time. The solution at the array surface is successively replaced by pumping five different water/ethylene glycol (EG) mixtures of decreasing ethylene glycol (EG) content (H_2O/EG (%) 99:1 to 100:0 (% vol)), which induces a decreasing of the refractive index n of the light scattering medium (from $n=$ 1.33279 RIU to 1.33168 RIU). Figure 5, which shows ΔE as a function of n, reveals that the intensity of the diffracted spot is directly proportional (linear fit with $R^2=0.9873$) to the bulk refractive index of the solution at the array surface. ΔE can thus be employed as the signal transduction for refractive index sensing. From the linear fit of Figure 5, a sensitivity of signal transduction $S=64.34\ \mathrm{V\,RIU^{-1}}$, defined by the slope and a refractive index resolution $R=1.30\times10^{-5}$ RIU, defined by the ratio between the standard deviation and the sensitivity, were extracted. This last value is on the same order of magnitude of the R values reported for most classical surface plasmon resonance (SPR) techniques.[41,42]

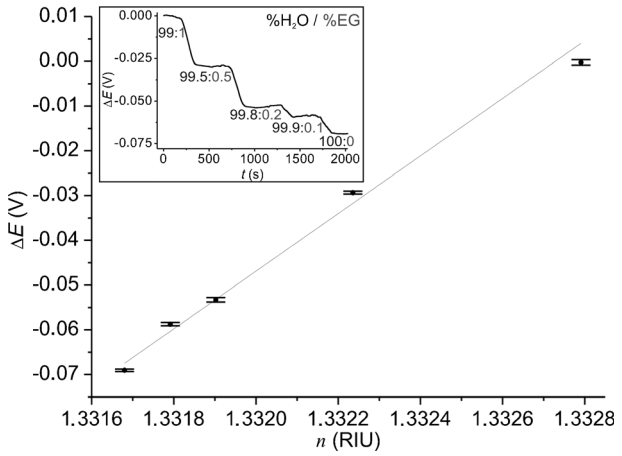

Figure 5. Plot of the difference of photodiode potential ΔE as a function of the refractive index of the solution injected in the flow cell n. Inset: detection curve showing the difference of photodiode potential as a function of time with different mixtures of water and ethylene glycol injected in the flow cell.

Monitoring of gold nanoparticles electrostatic adsorption

Having shown that changes in the bulk refractive index can be detected by using the SiO_2 NW arrays, we demonstrate that the diffraction at the SiO_2 NW arrays can also be used to detect in situ surface modifications of the SiO_2 NWs. In a proof-of-principle experiment, we monitored the electrostatic adsorption of a monolayer of negatively charged AuNPs (with a diameter of ca. 13 nm, concentration of 8 nM) on the SiO_2 NWs. The SiO_2 NWs were first modified with amino groups by silanization with (3-aminopropyl)trimethoxysilane (APTMS) to generate a positive surface charge. As illustrated in Figure 6a, the modified SiO_2 NWs immersed in water were exposed to negatively charged AuNPs (citrate stabilized), and the diffraction changes upon the in situ adsorption of the AuNPs onto the silica surface were monitored by diffraction. The adsorption curve is shown in Figure 6b, which shows the photodiode re-

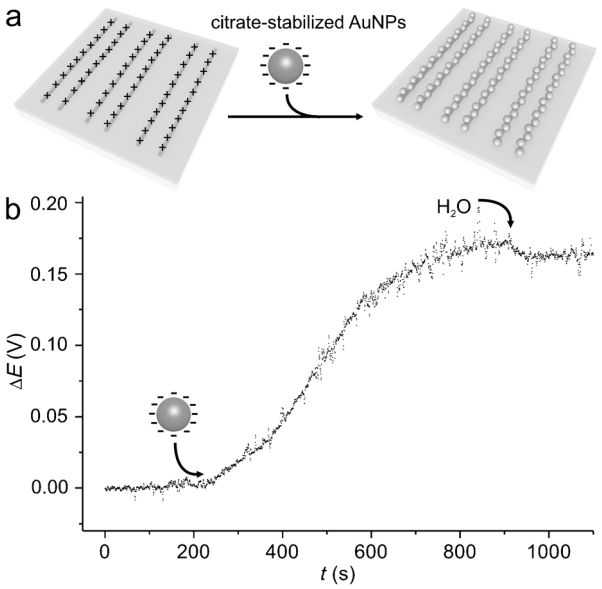

Figure 6. a) Scheme showing the in situ electrostatic adsorption of negatively charged gold nanoparticles on positively charged silica nanowires. b) Curve of the difference of photodiode potential as a function of the time showing the electrostatic adsorption of gold nanoparticles on silica nanowires.

sponse (ΔE) as a function of time. At 210 s, an aqueous dispersion of AuNPs was injected and an increase in ΔE from 0 to 170 mV was obtained due to the adsorption of AuNPs. Water was re-injected onto the array surface at 910 s, which induced a small decrease of the ΔE value to a constant value of 160 mV. This 10 mV decrease is attributed to the detachment of non-electrostatically bound AuNPs, which are removed from the silica surface upon rinsing. This experiment proves that surface modification can be also monitored based on the diffraction at the SiO_2 NW array surface.

Streptavidin adsorption on biotin-modified silica nanowires

In a second set of adsorption measurements, the SiO_2 NWs were toposelectively modified with biotin covalently, and these modified arrays were used to monitor the bioaffinity adsorption of a streptavidin monolayer. The covalent modification of the SiO_2 NWs with biotin was achieved by following a well-known procedure,[43] which involves first the modification of the silica surface with APTMS, and second the coupling of the amino groups with sulfo-NHS-biotin by the formation of an amide bond. As shown in Figure 7a, the biotin-modified SiO_2 NWs were then exposed to streptavidin. Streptavidin is a tetrameric protein which has four sites for binding biotin,[44] and the biotin–streptavidin bond is one of the strongest noncovalent interactions known, with a dissociation constant in the order of 10^{-14} M and a reported dissociation half-life of several days.[45] First, we observed the biotin-modified SiO_2 NWs after their exposure to a solution containing fluorophore-labeled streptavidin (Alexa647) by fluorescence microscopy. The inset of Figure 7b shows the fluorescence picture of the biotin-modified SiO_2 NWs after exposition to the fluorescent streptavidin. In this picture, the SiO_2 NWs are clearly revealed by their fluorescence as 700 nm-wide wires, which corresponds to the previous observations made with the optical microscope, as well as at the SEM. As a control experiment, SiO_2 NWs that were not modified with biotin were exposed to fluorescent streptavidin and observed under the fluorescence microscope. No observable fluorescence was detected in this case (as well as at the blank biotin-labeled SiO_2 NW array surface), which proves that no nonspecific interaction between the SiO_2 NW and streptavidin is responsible for the fluorescence response at the biotin-modified SiO_2 NW array surfaces. It can be concluded that streptavidin binds successfully and specifically to the biotin-modified SiO_2 NWs without yielding any nonspecific interaction with the underlying Cytop film.

After having shown that streptavidin specifically binds to biotin-modified SiO_2 NWs, we then demonstrated that it is possible to monitor the in situ attachment of streptavidin on biotin by using the array diffraction. First, phosphate buffered saline (PBS) was guided through the flow cell, and subsequently a 2.5 μM solution of streptavidin in PBS was injected on the array at 50 s. The detected development of the photodiode potential is shown in Figure 7b. The exposure of the biotin-modified SiO_2 NWs to streptavidin induces an immediate increase of ΔE that reaches its maximum of $\Delta E_{max} = 12$ mV at an incubation time of 200 s. The fact that this ΔE_{max} value is one order of magnitude lower than the one obtained before for the adsorption of a monolayer of AuNPs is attributed to the fact that the local refractive index change, which is induced by the protein layer, is much lower than the one that was previously obtained by the modification with AuNPs. The exposure of SiO_2 NWs, not modified with biotin to streptavidin provokes just a very slight increase of ΔE to a maximal value of $\Delta E_{max} = 0.6$ mV after an exposure time of 200 s (Figure 7b, grey curve). This value is less than 0.1% of the ΔE obtained with the biotin-modified SiO_2 NW array, which shows again the very low level of nonspecific adsorption of streptavidin onto the SiO_2 NWs.

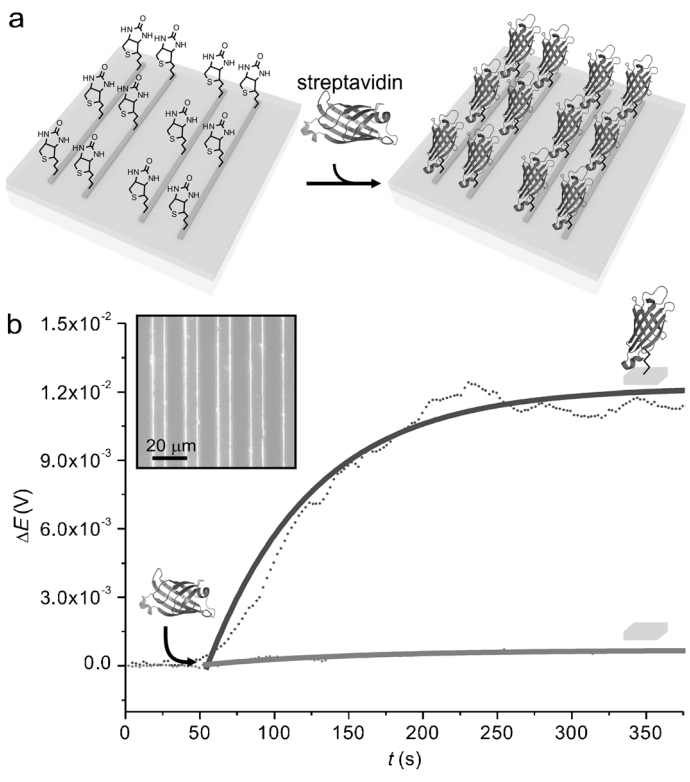

Figure 7. a) Scheme showing the attachment of streptavidin on biotin-functionalized silica nanowires. b) Binding curves of the interaction of streptavidin with biotin-functionalized silica nanowires (black) and with nonfunctionalized silica nanowires (grey). Dotted lines are the difference of photodiode potentials, and solid lines are the fits of the difference of photodiode potentials with kinetic equation (3). Inset: fluorescence microscopy image of silica nanowires functionalized with Alexa 647-tagged streptavidin.

Detection of thrombin with aptamer-functionalized silica nanowires

The SiO_2 NWs were functionalized with a ssDNA aptamer by using the poly(L-glutamic acid) (PGlu) attachment chemistry described recently,[46] and human α-thrombin was detected by using the diffraction of the aptamer-modified SiO_2 NWs. Thrombin is a serine protease, which catalyzes the conversion of soluble fibrinogen to insoluble fibrin,[47] and induces physiological and pathological blood coagulation. Although

a low level of thrombin promotes neuroprotection, it has been reported that thrombin concentrations above 50 nM can cause neuronal degeneration and even cell death.[48] Because of its implication in major pathologies,[49,50] it is of first importance to detect thrombin for medical diagnosis. Aptamers are specific dsDNA or ssDNA oligonucleotides that fold into well-defined three-dimensional structures and bind with specific targets.[51,52] Aptamers are designed for the recognition of a wide range of targets, such as proteins, peptides, and even cells with high affinity and specificity. The thrombin-binding 15-mer (5′-GGTTGGTGTGGTTGG-3′) was one of the first in vitro selected ssDNA aptamers targeted towards thrombin[53,54] and is now one of the most studied aptamers.[55] This aptamer has been previously used for the detection of thrombin with different techniques, such as colorimetry,[56] fluorescence,[57] SPR phase imaging,[58] electrochemistry,[59,60] and electrochemiluminescence.[61] Herein, we used this aptamer covalently attached to the SiO_2 NWs for the detection of human α-thrombin by diffraction.

The modification of the SiO_2 NWs surface with the thrombin-binding aptamer was performed as shown in Figure 8. The applied PGlu-based surface chemistry has been previously reported by our group,[46] and has been adapted herein to the modification of SiO_2 NWs. First, the surface of the SiO_2 NWs was activated by exposing the array surface to an oxygen plasma for a short time (20 s) to increase the number of silanol groups (Si–OH groups) on the silica surface. It is worth mentioning that no morphological change of the Cytop film was observed after this short plasma etching by SEM. Subsequently amino groups were introduced to the SiO_2 NWs by silanization with APTMS. PGlu, a polymer containing carboxylate groups was then electrostatically adsorbed onto the positively charged silica surface. Finally, the SiO_2 NWs were covalently modified with the PGlu backbone, as well as the thrombin-binding aptamer by the formation of amide bonds. This was achieved by incubation of a solution of the thrombin-binding aptamer coupled to an amino-terminated linker (ssDNA: 5′-$NH_2(CH_2)_6T_{15}$GGTTGGTGTGGTTGG-3′) and coupling agents 1-ethyl-3-[3-dimethylaminopropyl]carbodiimide hydrochloride (EDC) and *N*-hydroxysulfosuccinimide (sulfo-NHS) in PBS. This step yielded a surface of aptamer-modified SiO_2 NWs,[46] which is the final sensing platform demonstrated in this paper.

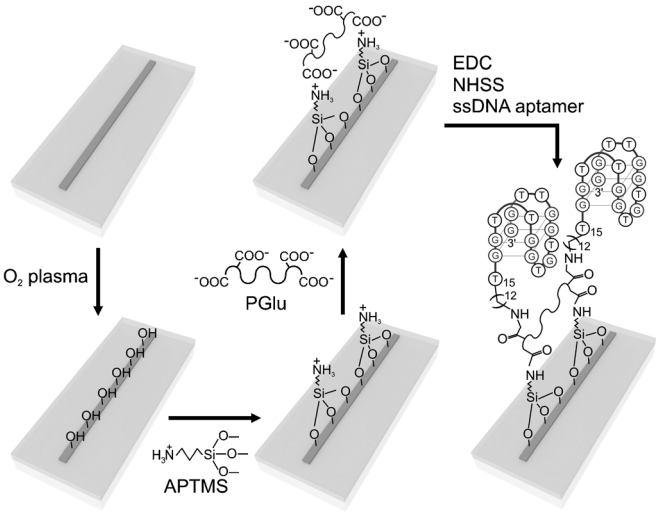

Figure 8. Scheme showing the functionalization of a silica nanowire with the thrombin binding ssDNA aptamer.

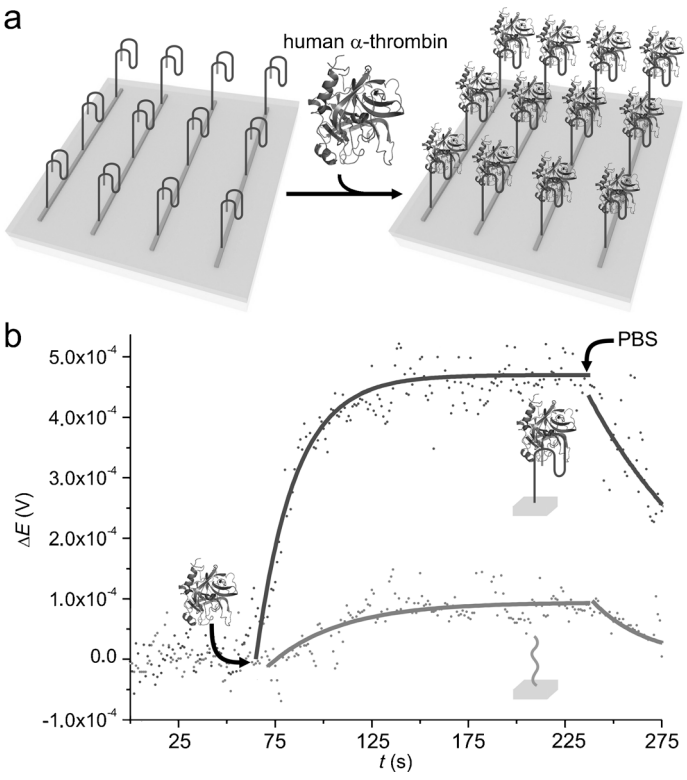

Figure 9. a) Scheme showing the binding of human α-thrombin on aptamer-functionalized silica nanowires. b) Binding curves of human α-thrombin on thrombin-binding aptamer-functionalized silica nanowires (black) and on T_{30}-funtionalized silica nanowires (grey). Dotted lines are the photodiode potentials shifts and solid lines are fits of equation (3) for the adsorption and (4) for the desorption.

The detection of human α-thrombin with the aptamer-modified SiO_2 NW array surfaces was studied by incubation of the sensing surface with a 30 mM target solution in PBS. As a control, this experiment was also performed with a SiO_2 NW array surface with a T_{30} ssDNA (5′-$NH_2(CH_2)_{12}T_{30}$-3′) instead of the thrombin-binding aptamer. Figure 9b shows the respective diffraction binding curves and reveals that the thrombin incubation of the aptamer-modified array surface induces an immediate increase of ΔE, which saturates at $\Delta E_{max} = 0.47$ mV after an incubation time of 140 s (Figure 9b, black dotted curve). In contrast, the exposition of the control array to the same concentration of thrombin only leads to an increase of ΔE_{max} of 0.09 mV (Figure 9b, grey dotted curve). This output signal is more than five times smaller than the signal obtained with the aptamer-modified array surface, and the increase in signal upon thrombin incubation is in this case attributed to nonspe-

cific adsorption of the protein onto the control T_{30} ssDNA-modified SiO_2 NWs. Figure 9b furthermore shows the fits of the two diffraction binding curves with the kinetic Equations (3) and (4) for the adsorption and the desorption processes, respectively (Figure 9b, black and grey solid lines).[62,63]

$$\Delta E = \frac{k_{on} C_{thr} \Delta E_{max}}{k_{on} C_{thr} + k_{off}} [1 - e^{-((k_{on} C_{thr} + k_{off})t)}] \quad (3)$$

$$\Delta E = \Delta E_0 e^{(-k_{off} t)} \quad (4)$$

in which C_{thr} is the concentration of the injected thrombin, ΔE_{max} is the maximum photodiode potential, and ΔE_0 is the photodiode potential at the beginning of the desorption. From the fit of the desorption part of the black curve of Figure 9b, the aptamer–thrombin dissociation rate constant, k_{off} was obtained. The association constant k_{on} was obtained from Equation (3) by using the calculated value for k_{off}. The ratio of these two constants k_{on}/k_{off} gives a Langmuir adsorption coefficient[62,63] $K_{ads} = 8.2 \times 10^7\ M^{-1}$, which is very close to previous values of K_{ads} obtained by SPR-based sensing techniques reported in the literature for comparable systems.[58,64] These diffraction experiments demonstrate that SiO_2 NW arrays can be reliably used for the diffraction detection of target proteins with a detection limit sufficiently low to allow the detection of pathologic concentrations of human α-thrombin, which should be of first importance for future applications in medical diagnosis.

Conclusion

A new technique based on a modified LPNE process involving the electrochemical sol–gel nanodeposition of silica for the fabrication of arrays of SiO_2 NWs with high aspect ratio and roughness on a fluoropolymer thin film was reported. We have shown their toposelective chemical modification and demonstrated their capability as a diffraction-based sensor by showing four different examples of detection involving bulk refractive-index sensing and sensing of nanoparticle and protein adsorption. In particular, we have shown that SiO_2 NWs functionalized with an ssDNA aptamer can be used for the detection of human α-thrombin below pathologic concentrations (30 nM). This fabrication technique could be employed for designing more complex arrays[8] that could be used for multiplexed detection. In addition to diffraction-based sensing, we believe that these SiO_2 NWs are promising for potential applications in the areas of photoluminescence[25–28] and waveguides[29–31] for microfluidic chips.

Experimental Section

Chemicals and materials

All the reagents were used as received. The photoresists: SU-8 5 and S1808, as well as the photoresist developers, were purchased from MicroChem. Cytop and the Cytop solvent were obtained from AGC. *N*-methylpyrrolidinone (NMP) and ethylene glycol (EG) were purchased from Fischer Scientific. 1-Ethyl-3-[3-dimethylaminopropyl]carbodiimide hydrochloride (EDC), *N*-hydroxysulfosuccinimide (sulfo-NHS), and sulfo-NHS-biotin were purchased from Thermo Scientific. Acetone was obtained from VWR, ethanol from Gold Shield, hydrochloric acid from J.T. Baker, and nitric acid from Macron Chemicals. PBS 10x was obtained from Affymetrix and diluted by ten with milliQ water prior to utilization. Hellmanex, tetraethyl orthosilicate (TEOS), sodium nitrate, (3-aminopropyl)trimethoxysilane (APTMS), and poly(L-glutamic acid) (PGlu; M_W = 50 000–100 000) were purchased from Sigma–Aldrich. The aqueous solutions were prepared by using milliQ water. The gold nanoparticles (AuNPs) were synthesized by using the known Turkevich method.[5] The amino-terminated ssDNA sequences were obtained from IDT. Alexa647-streptavidin was purchased from Molecular Probes, and human α-thrombin was obtained from Haematologic Technologies. The glass slides used for the deposition of Cytop were obtained from Fischer. The nickel pellets used for the thermal evaporation were purchased from Kurt J. Lesker.

Preparation of the silica sol

An aqueous solution of 0.1 M $NaNO_3$ (20 mL) was added to ethanol (20 mL). Under mechanical stirring and by using a pH meter (Oakton Instruments), the pH of the mixture was adjusted to a value of three by using a solution of HCl (0.1 M). TEOS (0.4 mL) was added to the mixture, and the solution was left under stirring for 6 h for hydrolyzing the TEOS.

Fabrication of the silica nanowire arrays

Glass slides (2.5×2.5 cm) were cleaned by ultrasonication in an aqueous solution of Hellmanex (1% vol), rinsed thoroughly with water and ethanol, and dried under a N_2 stream. The glass slides were then plasma cleaned under an oxygen plasma (Harrick PDC-32G) for 4 min. A solution of Cytop in solvent (1:5 (w/w)) was spin coated on the glass slide, and the glass slide was left for 1 h at 90° on a hot plate, and 1 h at 180° in the oven to evaporate the solvent. A layer of 170 nm of nickel was then deposited by vapor deposition (Denton DV 502 A evaporator) on the Cytop layer. SU-8 5 was spin coated on the nickel layer, soft baked on a hot plate, and the substrate was left for few hours, until it cooled to RT. The SU-8 5 photoresist was patterned with lines having a width of 10 μm and a respective spacing of 10 μm by using a mask aligner (Karl Suss MJB-3). The substrate was then post baked on the hot plate, left for few hours to cool to RT, developed by using the SU-8 developer, and rinsed under a N_2 stream. S1808 was spin coated on the Ni/SU-8 layer and the photoresist solvent was evaporated at 90° for 20 min in an oven. The positive photoresist was patterned with the mask aligner and developed (by using MF-319 developer) in such a way that the edges of the substrate were covered with the S1808 layer. The substrate was rinsed with water and dried under a N_2 flow. The nickel was etched by leaving the substrate in an aqueous solution of 0.8 M nitric acid for 14 min. After rinsing the surface thoroughly with water and drying it with an N_2 flow, an electrical contact area was made by dissolving a small part of the positive photoresist with acetone by using a Q-tip. The substrate was then connected to a potentiostat (PGSTAT12, Autolab) and used as a working electrode for the electrodeposition of silica in an O-ring electrochemical cell. The cell was filled with the silica sol, a platinum foil was used as a counterelectrode, and the deposition was achieved by chronoamperometry at −1.2 V vs. Ag/AgCl (3 M NaCl) for 70 s and rinsed with water. The surface was then rinsed with acetone and immersed for 15 min in *N*-methylpyrrolidinone,

which resulted in the dissolution of the positive photoresist and the removal of the negative photoresist. The nickel layer was totally etched away by immersing the substrate in nitric acid solution (2.7 M) for 30 min. The substrates were finally rinsed with water and dried with a N_2 flow.

Optical microscopy, fluorescence microscopy, and SEM characterization

The SiO_2 NWs were observed by using a Zeiss Axioskop 2 optical microscope. For the fluorescence microscopy, the biotin-modified SiO_2 NWs were exposed to a Alexa647-streptavidin solution (100 $\mu g\,mL^{-1}$) in PBS for 10 min in a humidity chamber. The surfaces were then rinsed with mQ water and dried with a N_2 flow. The imaging was performed by using an inverted microscope (Olympus IX71) with an Andor Neo scientific CMOS (South Windsor) camera. For the SEM characterization, a thin layer of iridium was previously sputtered by ion-beam-sputter deposition (IBS/e, South Bay Technology) on the surface to ensure a good electrical conduction. A Philips XL 30 was used for imaging the nanowires, and a FEI Magellan 400 XHR was used for the high magnification pictures.

Diffraction experiments

A flow cell was positioned on the array surface and the outer surface of the surface was coupled to a glass prism by using index-matching oil (Cargille). The array was positioned on a rotating stage to set the incident angle θ. The light was emitted by a $\lambda =$ 633 nm HeNe laser (JDSU), *p*-polarized by using a polarizer (Newport) and diffracted from the array surface. The buffer was passed through the array surface and the incident angle was set to the critical angle, so that the negative diffraction orders were in total internal reflection (TIR) geometry. For the photograph of Figure 4b, the diffraction pattern was projected on a black screen and photographed by using a Canon EOS 40D camera. In all the other experiments, the laser was chopped at a frequency of 1.0 kHz (Stanford Research Instruments SR540) and a photodiode (Hamamatsu) connected to a DSP lock-in amplifier (EG&G model 7220) was placed in front of the diffracted spots, the photodiode potential was recorded by a Labview program. For the intensity profile shown in Figure 4b, the photodiode was moved by using a rotating stage to screen the intensity of the diffraction spot. For all the other experiments, the photodiode was positioned on the diffracted spot having the highest intensity. After obtaining a stable background signal, the solutions containing a mixture of solvents (Figure 5, inset), gold nanoparticles in water (Figure 6b), or proteins in PBS 1x (Figures 7b and 9b) were injected through the flow cell.

Functionalization of the silica nanowires

For the functionalization of the SiO_2 NWs with amino groups, the array surface was first exposed to a 200 mT oxygen plasma (PDC-32G, Harrick Plasma) for 20 s and exposed for 2 h to a solution of APTMS (2% vol) in ethanol. The substrate was then rinsed with water and ethanol and dried under a N_2 flow. For the functionalization of the SiO_2 NWs with biotin, the amino-functionalized array was exposed to a solution of sulfo-NHS-biotin (5 mM) in PBS for 1 h, rinsed with water, and dried under a N_2 flow. For the functionalization of the SiO_2 NWs with ssDNA, the amino-functionalized array was exposed to a solution of PGlu (3 $mg\,mL^{-1}$) in PBS for 1 h, rinsed with water, dried under a N_2 flow, and exposed overnight to a PBS solution containing EDC (75 mM), sulfo-NHS (15 mM), and amino-terminated ssDNA (170 mM). The substrate was finally rinsed with water and dried under a N_2 stream. For the functionalization with the thrombin-binding aptamer, the ssDNA sequence 5′-$NH_2(CH_2)_6T_{15}$GGTTGGTGTGGTTGG-3′ was used, and for the control experiment shown in Figure 9b, the ssDNA sequence 5′-$NH_2(CH_2)_{12}T_{30}$-3′ was used.

Acknowledgements

This works was supported by the NIH grant R01-GM059622. The authors thank Dr. Nina Loget-Hüsken and Kyunghee Cho for valuable discussions, Dr. Aaron R. Halpern, and Dr. Mana Toma for helping with the optical set-up, Jennifer B. Wood for providing the gold nanoparticles, and Professor R. M. Penner for the use of his optical microscope. The Laboratory for Electron and X-ray Instrumentation (LEXI) is also acknowledged for the use of their SEMs.

Keywords: biosensors · electrodeposition · optical diffraction · silica nanowires · sol–gel processes

[1] F. Nakajima, Y. Hirakawa, T. Kaneta, T. Imasaka, *Anal. Chem.* **1999**, *71*, 2262 – 2265.
[2] Y. Han, R. M. Corn, *J. Phys. Chem. Lett.* **2011**, *2*, 1601 – 1606.
[3] R. C. Bailey, J. T. Hupp, *J. Am. Chem. Soc.* **2002**, *124*, 6767 – 6774.
[4] R. C. Bailey, J.-M. Nam, C. A. Mirkin, J. T. Hupp, *J. Am. Chem. Soc.* **2003**, *125*, 13541 – 13547.
[5] I. Sendroiu, R. Corn, *Biointerphases* **2008**, *3*, FD23 – FD29.
[6] Y. G. Tsay, C. I. Lin, J. Lee, E. K. Gustafson, R. Appelqvist, P. Magginetti, R. Norton, N. Teng, D. Charlton, *Clin. Chem.* **1991**, *37*, 1502 – 1505.
[7] F. Yu, S. Tian, D. Yao, W. Knoll, *Anal. Chem.* **2004**, *76*, 3530 – 3535.
[8] J. B. Goh, R. W. Loo, M. C. Goh, *Sens. Actuators B* **2005**, *106*, 243 – 248.
[9] P. M. St. John, R. Davis, N. Cady, J. Czajka, C. A. Batt, H. G. Craighead, *Anal. Chem.* **1998**, *70*, 1108 – 1111.
[10] M. G. Kang, L. J. Guo, *Adv. Mater.* **2007**, *19*, 1391 – 1396.
[11] G. Schider, J. R. Krenn, W. Gotschy, B. Lamprecht, H. Ditlbacher, A. Leitner, F. R. Aussenegg, *J. Appl. Phys.* **2001**, *90*, 3825.
[12] J. J. Yang, M. D. Pickett, X. Li, D. A. A. Ohlberg, D. R. Stewart, R. S. Williams, *Nat. Nanotechnol.* **2008**, *3*, 429 – 433.
[13] W. Yan, T. Ayvazian, J. Kim, Y. Liu, K. C. Donavan, W. Xing, Y. Yang, J. C. Hemminger, R. M. Penner, *ACS Nano* **2011**, *5*, 8275 – 8287.
[14] N. A. Melosh, A. Boukai, F. Diana, B. Gerardot, A. Badolato, P. M. Petroff, J. R. Heath, *Science* **2003**, *300*, 112 – 115.
[15] R. M. Penner, *Annu. Rev. Anal. Chem.* **2012**, *5*, 461 – 485.
[16] G. U. Kulkarni, B. Radha, *Nanoscale* **2010**, *2*, 2035 – 2044.
[17] J. A. Arter, D. K. Taggart, T. M. McIntire, R. M. Penner, G. A. Weiss, *Nano Lett.* **2010**, *10*, 4858 – 4862.
[18] R. Steve, P. Robert, *J. Micromech. Microeng.* **2001**, *11*, 287 – 300.
[19] A. E. Grigorescu, C. W. Hagen, *Nanotechnology* **2009**, *20*, 292001.
[20] G.-Y. Jung, Z. Li, W. Wu, S. Ganapathiappan, X. Li, D. L. Olynick, S. Y. Wang, W. M. Tong, R. S. Williams, *Langmuir* **2005**, *21*, 6127 – 6130.
[21] J. R. Heath, *Acc. Chem. Res.* **2008**, *41*, 1609 – 1617.
[22] E. J. Menke, M. A. Thompson, C. Xiang, L. C. Yang, R. M. Penner, *Nat. Mater.* **2006**, *5*, 914 – 919.
[23] C. Xiang, Y. Yang, R. M. Penner, *Chem. Commun.* **2009**, 859 – 873.
[24] A. R. Halpern, N. Nishi, J. Wen, F. Yang, C. Xiang, R. M. Penner, R. M. Corn, *Anal. Chem.* **2009**, *81*, 5585 – 5592.
[25] D. P. Yu, Q. L. Hang, Y. Ding, H. Z. Zhang, Z. G. Bai, J. J. Wang, Y. H. Zou, W. Qian, G. C. Xiong, S. Q. Feng, *Appl. Phys. Lett.* **1998**, *73*, 3076 – 3078.
[26] N. G. Shang, U. Vetter, I. Gerhards, H. Hofsäss, C. Ronning, M. Seibt, *Nanotechnology* **2006**, *17*, 3215 – 3218.
[27] C. L. Pang, H. Cui, C. X. Wang, *CrystEngComm* **2011**, *13*, 4082 – 4085.
[28] T. R. Alabi, D. Yuan, D. Bucknall, S. Das, *ACS Appl. Mater. Interfaces* **2013**, *5*, 8932 – 8938.
[29] L. Tong, R. R. Gattass, J. B. Ashcom, S. He, J. Lou, M. Shen, I. Maxwell, E. Mazur, *Nature* **2003**, *426*, 816 – 819.
[30] L. Tong, J. Lou, R. R. Gattass, S. He, X. Chen, Liu, E. Mazur, *Nano Lett.* **2005**, *5*, 259 – 262.

[31] L. Tong, L. Hu, J. Zhang, J. Qiu, Q. Yang, J. Lou, Y. Shen, J. He, Z. Ye, *Opt. Express* **2006**, *14*, 82 – 87.
[32] L. Gao, A. Ji, N. Lu, C. Li, Z. Cao, *AIP Adv.* **2012**, *2*, 012187.
[33] B. Zheng, Y. Wu, P. Yang, J. Liu, *Adv. Mater.* **2002**, *14*, 122 – 124.
[34] M. Zhang, Y. Bando, K. Wada, K. Kurashima, *J. Mater. Sci.* **1999**, *18*, 1911 – 1913.
[35] A. Walcarius, E. Sibottier, M. Etienne, J. Ghanbaja, *Nat. Mater.* **2007**, *6*, 602 – 608.
[36] F. Qu, R. Nasraoui, M. Etienne, Y. B. S. Côme, A. Kuhn, J. Lenz, J. Gajdzik, R. Hempelmann, A. Walcarius, *Electrochem. Commun.* **2011**, *13*, 138 – 142.
[37] H. Lalo, Y. Bon-Saint-Côme, B. Plano, M. Etienne, A. Walcarius, A. Kuhn, *Langmuir* **2012**, *28*, 2323 – 2326.
[38] G. Loget, J. Roche, E. Gianessi, L. Bouffier, A. Kuhn, *J. Am. Chem. Soc.* **2012**, *134*, 20033 – 20036.
[39] O. Lev, Z. Wu, S. Bharathi, V. Glezer, A. Modestov, J. Gun, L. Rabinovich, S. Sampath, *Chem. Mater.* **1997**, *9*, 2354 – 2375.
[40] P. M. Dentinger, W. M. Clift, S. H. Goods, *Microelectron. Eng.* **2002**, *61 – 62*, 993 – 1000.
[41] J. Homola, S. S. Yee, G. Gauglitz, *Sens. Actuators B* **1999**, *54*, 3 – 15.
[42] I. Stemmler, A. Brecht, G. Gauglitz, *Sens. Actuators B* **1999**, *54*, 98 – 105.
[43] R. Karnik, K. Castelino, C. Duan, A. Majumdar, *Nano Lett.* **2006**, *6*, 1735 – 1740.
[44] P. Weber, D. Ohlendorf, J. Wendoloski, F. Salemme, *Science* **1989**, *243*, 85 – 88.
[45] N. M. Green in *Methods in Enzymology, Vol. 184* (Eds.: W. Meir, A. B. Edward), Academic Press, Waltham (USA), **1990**, pp. 51 – 67.
[46] Y. Chen, A. Nguyen, L. Niu, R. M. Corn, *Langmuir* **2009**, *25*, 5054 – 5060.
[47] W. Bode, I. Mayr, U. Baumann, R. Huber, S. R. Stone, J. Hofsteenge, *EMBO J.* **1989**, *8*, 3467 – 3475.
[48] F. Striggow, M. Riek, J. Breder, P. Henrich-Noack, K. G. Reymann, G. Reiser, *Proc. Natl. Acad. Sci. USA* **2000**, *97*, 2264 – 2269.
[49] A. Nishino, M. Suzuki, H. Ohtani, O. Motohashi, K. Umezawa, H. Nagura, T. Yoshimoto, *J. Neurotrauma* **1993**, *10*, 167 – 179.
[50] T. Arai, J. Miklossy, A. Klegeris, J.-P. Guo, P. L. McGeer, *J. Neuropathol. Exp. Neurol.* **2006**, *65*, 19 – 25.
[51] E. J. Cho, J.-W. Lee, A. D. Ellington, *Annu. Rev. Anal. Chem.* **2009**, *2*, 241 – 264.
[52] A. D. Keefe, S. Pai, A. Ellington, *Nat. Rev. Drug. Discovery* **2010**, *9*, 537 – 550.
[53] L. C. Bock, L. C. Griffin, J. A. Latham, E. H. Vermaas, J. J. Toole, *Nature* **1992**, *355*, 564 – 566.
[54] K. Padmanabhan, K. P. Padmanabhan, J. D. Ferrara, J. E. Sadler, A. Tulinsky, *J. Biol. Chem.* **1993**, *268*, 17651 – 17654.
[55] M. C. R. Buff, F. Schäfer, B. Wulffen, J. Müller, B. Pötzsch, A. Heckel, G. Mayer, *Nucleic Acids Res.* **2010**, *38*, 2111 – 2118.
[56] H.-A. Ho, M. Leclerc, *J. Am. Chem. Soc.* **2004**, *126*, 1384 – 1387.
[57] N. Li, C.-M. Ho, *J. Am. Chem. Soc.* **2008**, *130*, 2380 – 2381.
[58] W.-J. Zhou, A. R. Halpern, T. H. Seefeld, R. M. Corn, *Anal. Chem.* **2011**, *83*, 440 – 445.
[59] Y. Xiao, A. A. Lubin, A. J. Heeger, K. W. Plaxco, *Angew. Chem.* **2005**, *117*, 5592 – 5595; *Angew. Chem. Int. Ed.* **2005**, *44*, 5456 – 5459.
[60] A.-E. Radi, J. L. Acero Sánchez, E. Baldrich, C. K. O'Sullivan, *J. Am. Chem. Soc.* **2005**, *127*, 117 – 124.
[61] Z. Lin, L. Chen, X. Zhu, B. Qiu, G. Chen, *Chem. Commun.* **2010**, *46*, 5563 – 5565.
[62] P.-H. Lin, R.-H. Chen, C.-H. Lee, Y. Chang, C.-S. Chen, W.-Y. Chen, *Colloids Surf. B* **2011**, *88*, 552 – 558.
[63] L. K. Wolf, Y. Gao, R. M. Georgiadis, *J. Am. Chem. Soc.* **2007**, *129*, 10503 – 10511.
[64] Y. Chen, K. Nakamoto, O. Niwa, R. M. Corn, *Langmuir* **2012**, *28*, 8281 – 8285.

Received: December 7, 2013
Published online on March 3, 2014

